Influence of entrance channel on the production of hassium isotopes

Juhee Hong
Rare Isotope Science Project, Institute for Basic Science, Daejeon 305-811, Korea

G. G. Adamian and N. V. Antonenko
Joint Institute for Nuclear Research, Dubna 141980, Russia
(Received 5 June 2015; published 17 July 2015)

The production of hassium isotopes $^{266-271}$Hs in various reactions ^{22}Ne + ^{249}Cf, ^{25,26}Mg + ^{248}Cm, ^{30}Si + ^{244}Pu, ^{34,36}S + ^{238}U, ^{40}Ar + ^{232}Th, and ^{48}Ca + ^{226}Ra is studied within the dinuclear system model. The experimental excitation functions of the isotopes $^{266-271}$Hs are well described and predictions are made for future experiments.

DOI: 10.1103/PhysRevC.92.014617 PACS number(s): 25.70.Hi, 24.10.−i, 24.60.−k

I. INTRODUCTION

Heavy-ion fusion reactions have been extensively used to produce superheavy elements (SHEs) in the actinide-based [1–3] and Pb- and Bi-based [4–9] complete fusion reactions at Flerov Laboratory of Nuclear Reactions (Dubna), GSI (Darmstadt), Rikagaku Kenkyusho (RIKEN, The Institute of Physical and Chemical Research) (Tokyo), Lawrence Berkeley National Laboratory (Berkeley), Grand Accelerateur National d'Ions Lourds (Caen), and Institute of Modern Physics (Lanzhou). The investigation of transfermium elements expands our knowledge of the single-particle structure, location of the shell closures, and decay modes of heaviest nuclei. For example, the predictions of deformed subshell with $Z = 108$ and $N = 162$ by macroscopic-microscopic models [10,11] have been experimentally confirmed [12].

The measurement and prediction of reaction cross sections is the most important task in the studies of SHE. In addition to ^{269}Hs studied in the α-decay chain of the ^{277}112 nucleus [13], the isotopes of hassium [$^{267-271}$Hs] have been synthesized in several experiments [3,14–17]. The remarkable result was the observation of the $3n$ evaporation channel in the ^{26}Mg + ^{248}Cm reaction at sub-barrier energies. The measured cross section was unexpectedly large, almost comparable to those in the $4n$ and $5n$ evaporation channels within the experimental uncertainties. The ratio between the cross sections in different fusion-evaporation channels is important for the correct identification of each isotope by α decay or spontaneous fission. Indeed, the excitation functions in the neighboring evaporation channels can be considerably overlapped.

The sub-barrier fusion at energy below the Coulomb barrier and the entrance-channel effects in the fusion process are not completely understood [18–23]. The calculation of the evaporation residue cross sections in the xn ($x \leqslant 4$) evaporation channels demands an accurate treatment of the capture probability in the entrance channel because the collision occurs at energies near the Coulomb barrier and the effect of the mutual orientation of colliding nuclei should be taken into consideration. In this respect the accurate treatment of the fusion probabilities is necessary as well. To investigate the influence of the entrance channels, we consider the dinuclear system (DNS) model [24,25], which describes the production of nearby isotopes in a consistent way. We then apply the model to describe the yields of Hs isotopes produced in various fusion reactions. By comparing with the existing experimental data, we adjust several free parameters and make predictions for the unexplored reaction channels.

The purpose of this work is to study near- and sub-barrier fusion reactions leading to the production of hassium isotopes. The effect of the entrance channel will be investigated. In Sec. II, we discuss the DNS model to describe near- and sub-barrier fusion. This model is used in Sec. III to calculate the production cross sections of Hs isotopes in the various entrance channels. For the $3n$-$5n$ evaporation channels, we analyze all the evaporation residue cross sections and compare them with existing experimental data. Finally, we summarize our results in Sec. IV.

II. NEAR- AND SUB-BARRIER FUSION

In this section, we discuss the DNS model to describe near- and sub-barrier fusion. The DNS has two main degrees of freedom: the mass asymmetry coordinate $\eta = (A_1 - A_2)/(A_1 + A_2)$ and the relative distance between the centers of mass of nuclei R [24,25]. After the system is captured in a pocket of the nucleus-nucleus potential at $R = R_m$, the relative kinetic energy is transferred into the potential and excitation energy. The DNS develops in time by diffusion in the mass asymmetry coordinate η. The potential energy of the DNS,

$$U(R_m,\eta,\beta_i,J) = B_1 + B_2 + V(R_m,\eta,\beta_i,J) - \left[B_{12} + E_{12}^{\rm rot}(J)\right], \quad (1)$$

is calculated with respect to the potential energy $B_{12} + E_{12}^{\rm rot}(J)$ [B_{12} is the mass excess of the compound nucleus (CN) and $E_{12}^{\rm rot}(J)$ is the rotational energy of the CN] of the rotational CN. The nucleus-nucleus interaction potential is

$$V = V_N + V_C + V_R$$

and B_1 and B_2 are the mass excesses of fragments in their ground states. The microscopical effects are taken into account through the experimental and theoretical mass excesses of the DNS nuclei. For the deformed interacting nuclei [$\beta_i (i = 1,2)$ are the quadrupole deformation parameters of nuclei], the Coulomb potential is [26]

$$V_C = \frac{e^2 Z_1 Z_2}{R} + \frac{3}{5}\frac{e^2 Z_1 Z_2}{R^3}\sum_{i=1,2} R_{0i}^2 \beta_i Y_{20}(\theta_i), \quad (2)$$

where $R_{0i} = r_0 A_i^{1/3}$ fm ($i = 1,2$) and $r_0 = 1.15$ fm. For the nuclear part,

$$V_N = \int \rho_1(\mathbf{r_1})\rho_2(\mathbf{R}-\mathbf{r_2})F(\mathbf{r_1}-\mathbf{r_2})d\mathbf{r_1}d\mathbf{r_2}, \quad (3)$$

of the nucleus-nucleus potential, we use the double-folding procedure with the Skyrme-type density-depending effective nucleon-nucleon interaction,

$$F(\mathbf{r_1}-\mathbf{r_2}) = C_0\left\{F_{\rm in}\frac{\rho_0(\mathbf{r_1})}{\rho_{00}} + F_{\rm ex}\left[1-\frac{\rho_0(\mathbf{r_1})}{\rho_{00}}\right]\right\}\delta(\mathbf{r_1}-\mathbf{r_2}), \quad (4)$$

which is known from the theory of finite Fermi systems [27], and $\rho_0(\mathbf{r}) = \rho_1(\mathbf{r}) + \rho_2(\mathbf{R}-\mathbf{r})$ and $F_{\rm in,ex} = f_{\rm in,ex} + f'_{\rm in,ex}\frac{(N_1-Z_1)(N_2-Z_2)}{(N_1+Z_1)(N_2+Z_2)}$. Here $\rho_1(\mathbf{r_1})$ and $\rho_2(\mathbf{r_2})$ and N_2 (Z_2) are the nucleon densities of, respectively, the light and the heavy nuclei of the DNS and neutron (charge) number of the heavy nucleus of the DNS. Our calculations are performed with the following set of parameters: $C_0 = 300$ MeV fm^3, $f_{\rm in} = 0.09$, $f_{\rm ex} = -2.59$, $f'_{\rm in} = 0.42$, $f'_{\rm ex} = 0.54$, and $\rho_{00} = 0.17$ fm^{-3} [28]. The densities of the nuclei are taken in the two-parameter Woods-Saxon form with the nuclear radius parameter $r_0 = 1.15$ fm and the diffuseness parameter $a = 0.55$ fm [28]. The centrifugal potential is

$$V_R = \hbar^2 J(J+1)/(2\Im),$$

where the moment of inertia $\Im$ of the DNS formed is calculated in the sticking limit as $\Im = \Im_1 + \Im_2 + \mu R_m^2$, where the moments of inertia $\Im_i$ ($i = 1,2$) of the DNS nuclei are obtained in the rigid-body approximation. Calculating the nucleus-nucleus potential in the DNS, we find R_m at which the potential pocket has a minimum [25,28]. The value of R_m is about 0.5 fm larger than the distance between the centers of nuclei at touching. When the nucleus-nucleus potential is calculated in the entrance channel (the capture stage), the value of the moment of inertia is replaced with $\Im = \mu R^2$.

The evaporation residue cross section in the xn evaporation channel can be written as a sum over partial contributions [24,25,29],

$$\sigma_{xn}(E_{\rm c.m.}) = \sum_{J=0}^{J_{\max}} \sigma_{\rm cap}(E_{\rm c.m.},J)P_{\rm CN}(E_{\rm c.m.},J)W_{xn}(E_{\rm c.m.},J). \quad (5)$$

The factors are the partial capture cross sections, the fusion $P_{\rm CN}$, and survival W_{xn} probabilities. Because the considered incident energies are near the Coulomb barrier, the contributing angular momenta in σ_{xn} are limited by the kinematic [30] or by the survival probability of the highly fissile SHE. Using the experimental data on the population of the rotational states in ^{254}No [31], we set $J_{\max} = 10$ as in Ref. [25]. The same constant value of $J_{\max}$ one can use at sub-barrier energies [30]. Introducing the dependence of W_{xn} on J and taking the weak dependence of $P_{\rm CN}$ on J at $J < 25$ into account [32], we approximate the evaporation residue cross section by Eq. (6) The reduction of J dependence of σ_{xn} into the effective capture cross section is rather standard in the region of heavy nuclei [33]. We approximate the evaporation residue cross section by

$$\sigma_{xn}(E_{\rm c.m.}) = \sigma_{\rm cap}^{\rm eff}(E_{\rm c.m.})P_{\rm CN}(E_{\rm c.m.})W_{xn}(E_{\rm c.m.}), \quad (6)$$

with the reduced to $J = 0$ probabilities $P_{\rm CN}(E_{\rm c.m.}) = P_{\rm CN}(E_{\rm c.m.},J=0)$, $W_{xn}(E_{\rm c.m.}) = W_{xn}(E_{\rm c.m.},J=0)$, and an effective capture cross section

$$\sigma_{\rm cap}^{\rm eff}(E_{\rm c.m.}) = \frac{\pi\hbar^2}{2\mu E_{\rm c.m.}}\sum_{J=0}^{J_{\max}}(2J+1)T_J(E_{\rm c.m.}). \quad (7)$$

Here $\mu = m_0\frac{A_1A_2}{A_1+A_2}$ is the reduced mass (m_0 is the nucleon mass). For the nucleus-nucleus interaction potential approximated by an inverted harmonic oscillator with frequency ω_B and barrier height V_B and position R_B, the transmission coefficient T_J is given by the well-known Hill-Wheeler-type formula [34],

$$T_J(E_{\rm c.m.}) = \frac{1}{1+\exp\left[2\pi\left\{V_B+\hbar^2J(J+1)/2\mu R_B^2 - E_{\rm c.m.}\right\}/\hbar\omega_B\right]}. \quad (8)$$

Replacing the sum with the integral in Eq. (7), employing Eq. (8), and integrating over J, we obtain the effective capture cross section

$$\sigma_{\rm cap}^{\rm eff}(E_{\rm c.m.}) = \frac{\pi\hbar^2J_{\max}^2}{2\mu E_{\rm c.m.}}\left(1+\frac{\mu_0}{\zeta}\ln\{1+\exp[\alpha(V_B-E_{\rm c.m.})]\} - \frac{\mu_0}{\zeta}\ln\{1+\exp[\alpha(V_B-E_{\rm c.m.})+\zeta/\mu_0]\}\right). \quad (9)$$

Here $\mu_0 = A_1A_2/(A_1+A_2)$, $\alpha = \frac{2\pi}{\hbar\omega_B}$, and $\zeta = \frac{\pi\hbar^2J_{\max}^2}{m_0\hbar\omega_BR_B^2}$. Because the Coulomb barrier height V_B generally depends on the orientation of the colliding deformed nuclei, the effective capture cross section should take into account all possible orientations of nuclei. Instead of such direct calculation we consider the orientation effect effectively, through V_B, ζ, and α. In the calculations we employed the formula (9), where V_B defines the Coulomb barrier for the side-by-side orientation of the nuclei, $\zeta = 41.47$, and $\alpha = 0.5$. We adjusted these parameters to compare with the existing experimental data for the reactions ^{26}Mg + ^{248}Cm $\rightarrow$ $^{274-xn}$Hs + xn (x = 3–5). All calculations below are performed with the same set of parameters. The values of V_B and $V_B^{\rm sp} = V(R_B,\eta,\beta_i = 0, J = 0)$ are listed in Table I for the reactions considered.

The initially formed DNS with $\eta = \eta_i$ is usually in the local potential minimum in the mass asymmetry coordinate. In the DNS model, the fusion occurs in mass asymmetry coordinates towards the one-body shape (CN) [25]. As shown [25], the fusion in η is the most probable path in the reactions with massive nuclei. The DNS model was well tested many times. In the present paper we only apply this model to specific reactions. The fusion probability $P_{\rm CN}$ gives the probability that the DNS crosses the inner fusion barrier (with the barrier height $B^*_{\rm fus}$) in η and forms the CN. The symmetrization barrier (with the barrier height $B^{\eta}_{\rm qf}$) in the driving potential (1) is situated behind the initial mass fragmentation η_i toward smaller values

TABLE I. The Coulomb barrier $V_B^{\rm sp}$ for the spherical nuclei, the Coulomb barrier V_B for the side-by-side orientation of nuclei, the Q value for complete fusion, the excitation energy $V_B^{\rm sp}+Q$ of the CN at incident energy $E_{\rm c.m.}=V_B^{\rm sp}$, and the excitation energy V_B+Q of the CN at incident energy $E_{\rm c.m.}=V_B$ for the indicated reaction.

Reaction	Q (MeV)	$V_B^{\rm sp}$ (MeV)	$V_B^{\rm sp}+Q$ (MeV)	V_B (MeV)	V_B+Q (MeV)
^{22}Ne + ^{249}Cf	− 63.9	103.7	39.8	109.5	45.6
^{25}Mg + ^{248}Cm	− 75.4	121.8	46.4	128.5	53.1
^{26}Mg + ^{248}Cm	− 80.0	121.3	41.3	127.5	47.5
^{30}Si + ^{244}Pu	− 95.8	138.2	42.4	144.6	48.8
^{34}S + ^{238}U	− 109.3	154.5	45.2	159.9	50.6
^{36}S + ^{238}U	− 114.5	153.5	39.0	158.9	44.4
^{40}Ar + ^{232}Th	− 126.3	168.9	42.6	177.1	50.8
^{48}Ca + ^{226}Ra	− 151.3	181.6	30.3	185.9	34.6
^{26}Mg + ^{238}U	− 74.0	116.9	42.9	122.7	48.7

of η, $|\eta|<|\eta_i|$, and hinders the DNS to proceed to more symmetric configurations. The DNS can decay in two ways, namely in R from the initial configuration by the overcoming the quasifission barrier (with the barrier height $B_{\rm qf}^R$) or can first evolve (by overcoming the symmetrization barrier) to more symmetric configurations from which it decays in R with a larger probability because of the larger Coulomb repulsion. To calculate $P_{\rm CN}$, in Ref. [29] we suggested the approximate expression

$$P_{\rm CN}(E^*_{\rm CN})=\frac{1.25\,\exp[-(B^*_{\rm fus}-B_{\rm qf})/T_{\rm DNS}]}{1+1.25\,\exp[-(B^*_{\rm fus}-B_{\rm qf})/T_{\rm DNS}]}, \quad (10)$$

where $B_{\rm qf}=\min[B_{\rm qf}^R,B_{\rm qf}^\eta]$ is the minimum decay barrier height, $E^*_{\rm CN}=E_{\rm c.m.}+Q$ is the excitation energy of the CN, $T_{\rm DNS}=\sqrt{[E^*_{\rm CN}-U(R_m,\eta_i,\beta_i,J=0)]/a}$ is the temperature of the initial DNS, and $a=A/10$ MeV^{-1} is the level density parameter. As follows from our calculations, Eq. (10) supplies a good approximation of fusion probabilities. The heights of the barriers are strongly influenced by shell and deformation effects. The details of calculations of the barriers are presented in Refs. [24,25,29].

The value of the survival probability under the evaporation of x neutrons is defined as [35,36]

$$W_{xn}(E^*_{\rm CN})=P_{xn}(E^*_{\rm CN})\prod_{i=1}^{x}\frac{\Gamma_n\left(E^*_{{\rm CN}_i}\right)}{\Gamma_f\left(E^*_{{\rm CN}_i}\right)+\Gamma_n\left(E^*_{{\rm CN}_i}\right)}. \quad (11)$$

Here i, $E^*_{{\rm CN}_i}$, P_{xn}, and Γ_f (Γ_n) are the index of the evaporation step, the mean value of excitation energy in the evaporation step "i", the probability of realization of the xn channel at the initial excitation energy $E^*_{\rm CN}$ of the CN, and the width of fission (neutron evaporation), respectively. At the first step $i=1$ and $E^*_{{\rm CN}_1}=E^*_{\rm CN}$. In the SHE at considered excitation energies ($E^*_{\rm CN}$ is much larger than the neutron separation energy) the emission of γ rays and charged particles are much less probable than the neutron emission. The emission of charged particles is suppressed by the large Coulomb barrier and the emission of γ rays plays a role only at smaller $E^*_{\rm CN}$. Under these circumstances the total width of the CN decay is the sum of partial widths of neutron evaporation Γ_n and fission Γ_f. Therefore, the survival probability W_{xn} reflects the competition between the neutron evaporation and fission of the excited CN. Because in the considered nuclei $\Gamma_n\ll\Gamma_f$, $\Gamma_n/(\Gamma_n+\Gamma_f)\approx\Gamma_n/\Gamma_f$. With the level densities [37] of the Fermi-gas model, this ratio is

$$\frac{\Gamma_n}{\Gamma_f}=\frac{4A^{2/3}a_f[E^*_{\rm CN}-B_n]}{ka_n\{2\sqrt{a_f[E^*_{\rm CN}-B_f(E^*_{\rm CN})]}-1\}}\times\exp\{2\sqrt{a_n[E^*_{\rm CN}-B_n]}-2\sqrt{a_f[E^*_{\rm CN}-B_f(E^*_{\rm CN})]}\}, \quad (12)$$

where $k=9.8$ MeV, B_n is the neutron separation energy, $a_n=a$, and the ratio of the level density parameters in the fission and neutron evaporation channels is equal to $a_f/a=1.04$. The fission barrier B_f has the liquid-drop and microscopical parts, $B_f^{\rm LD}$ and $B_f^{\rm M}(E^*_{\rm CN})$, respectively: $B_f(E^*_{\rm CN})=B_f^{\rm LD}+B_f^{\rm M}(E^*_{\rm CN})$. The liquid drop part is calculated as in Ref. [38]. For example, for the considered isotopes of Hs, $B_f^{\rm LD}$ is about 0.2 MeV. The value $B_f^{\rm M}=\delta W_{\rm sd}-\delta W_{\rm gr}$ is the difference between the shell correction $\delta W_{\rm sd}$ of the nucleus at the saddle point and the shell correction $\delta W_{\rm gr}$ of the nucleus in the ground state. Usually, one neglects the shell correction at the saddle point, $\delta W_{\rm sd}\approx 0$ and, thus, $B_f^{\rm M}=|\delta W_{\rm gr}|$. Owing to the dependence of the shell effects on the nuclear excitation, the value of B_f effectively depends on $E^*_{\rm CN}$ as

$$B_f(E^*_{\rm CN})=B_f^{\rm LD}+B_f(E^*_{\rm CN}=0)\exp[-E^*_{\rm CN}/E_d],$$

where the damping factor is $E_d=25$ MeV. The pairing corrections $\delta=22/\sqrt{A}$, $11/\sqrt{A}$, and 0 for even-even, even-odd, and odd-odd nuclei, respectively, were regarded as follows: $E^*_{\rm CN}-B_j\to E^*_{\rm CN}-B_j-\delta$, where $j=n,f$, in Eq. (12). The neutron binding energies B_n and the microscopic corrections $\delta W_{\rm gr}^{\rm mc}$ are taken from Ref. [39]. To avoid a double counting of pairing in the fission barrier which is purely the shell correction, $B_f^{\rm M}=|\delta W_{\rm gr}|=|\delta W_{\rm gr}^{\rm mc}|-\delta$. The probability of realization of the xn channel at the initial excitation energy $E^*_{\rm CN}$ is

$$P_{xn}(E^*_{\rm CN})=P[x]-P[x+1], \quad (13)$$

where

$$P[x]=1-\exp[-\Delta_x/T]\left[1+\sum_{i=1}^{2x-3}\frac{(\Delta_x/T)^i}{i!}\right], \quad (14)$$

with

$$\Delta_x=E^*_{\rm CN}-\sum_{i=1}^{x}B_n(i) \quad (15)$$

and the average temperature

$$T=\sqrt{E^*_{\rm CN}/(2a)}. \quad (16)$$

The $B_n(i)$ is the neutron binding energy in the evaporation step "i". The values of W_{xn} obtained with this procedure are very close to those calculated with the statistical code GROGIF [29].

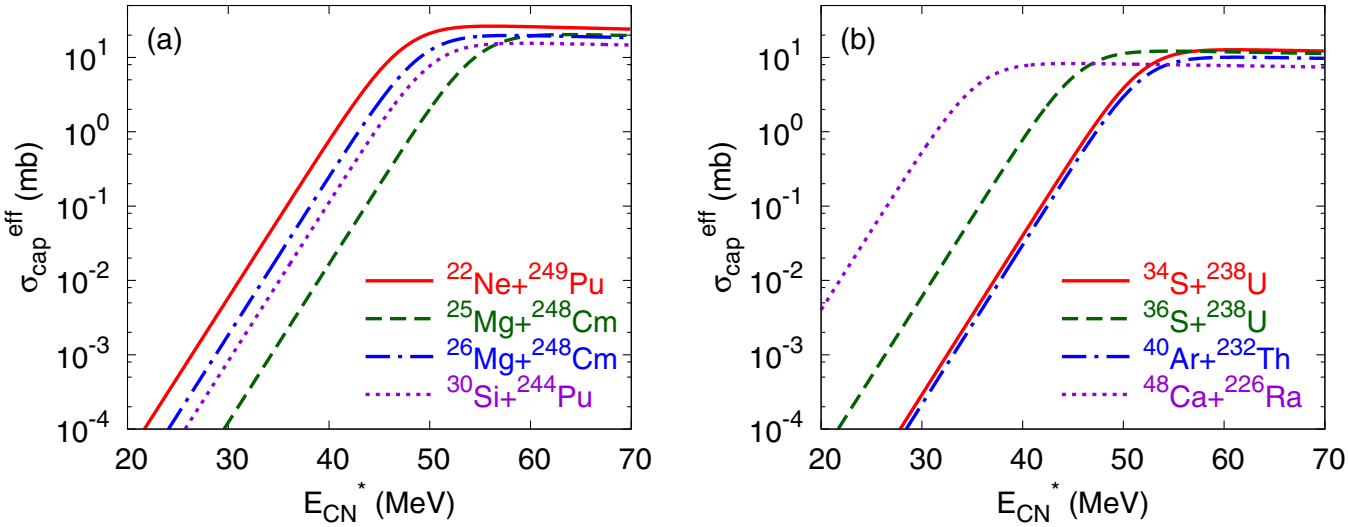

FIG. 1. (Color online) The calculated dependence of the effective capture cross section on the excitation energy of the CN for the indicated reactions.

III. CALCULATED RESULTS AND DISCUSSIONS

The model of the previous section is used to calculate the production cross section of the hassium isotopes in the complete fusion reactions ^{22}Ne + ^{249}Cf, ^{25,26}Mg + ^{248}Cm, ^{30}Si + ^{244}Pu, ^{34,36}S + ^{238}U, ^{40}Ar + ^{232}Th, and ^{48}Ca + ^{226}Ra with different entrance-channel charge (mass) asymmetries. For the Hs isotopes, the several sets of experimental data are available nowadays [3,14–17].

Figures 1(a) and 1(b) show the effective capture cross section as a function of the excitation energy of the CN. As the energy increases, the capture cross section increases at low energy and then reaches the maximum at energy around $E^*_{CN} = V_B + Q$. Because the reactions ^{48}Ca + ^{226}Ra have the lowest $E^*_{CN} = V_B + Q$ [mainly owing to the large negative Q value] compared to other reactions forming ^{274}Hs*, the effective capture cross section is relatively larger at energies below the Coulomb barrier for the spherical nuclei (see Table I). As a result, in this reaction one can expect the largest evaporation residue cross section in $3n$ or $4n$ channels.

In very asymmetric DNS ^{22}Ne + ^{249}Cf, ^{25,26}Mg + ^{248}Cm, and ^{30}Si + ^{244}Pu, the fusion probabilities P_{CN} are in the interval 0.8–1.0. In these reactions, the fusion barrier height is smaller than the quasifission barrier height ($B^*_{fus} < B_{qf}$) and the fusion probability slightly decreases as energy grows and approaches unity with decreasing energy. For more symmetric reactions ^{34,36}S + ^{238}U, ^{40}Ar + ^{232}Th, and ^{48}Ca + ^{226}Ra in which $B^*_{fus} > B_{qf}$, the fusion probability is smaller and increases with excitation energy (Fig. 2). Thus, the reactions with

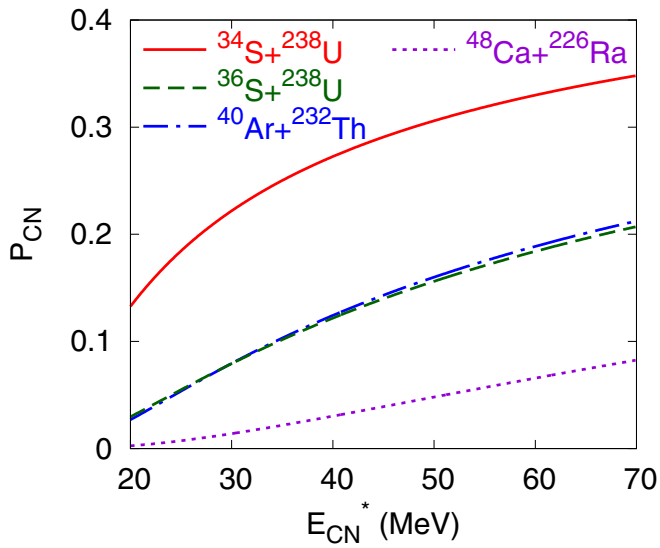

FIG. 2. (Color online) The calculated dependence of the fusion probability on the excitation energy of the CN for the indicated reactions.

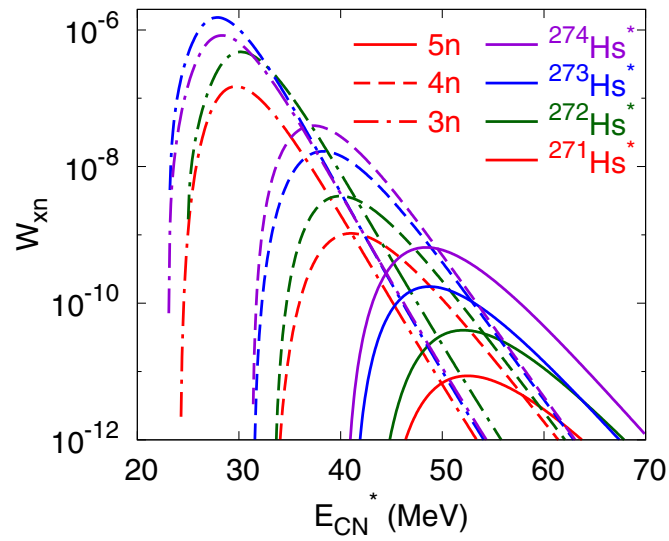

FIG. 3. (Color online) The calculated survival probabilities as functions of the CN excitation energy. The CN are indicated by various colors. The solid, dashed, and dash-dotted lines are for the $5n$, $4n$, and $3n$ channels, respectively.

larger charge and mass asymmetries are more favorable for fusion than those with smaller charge and mass asymmetries.

Figure 3 shows the survival probabilities of the CN $^{271-274}$Hs*. The transition from xn evaporation channel to $(x-1)n$ leads to the increase of the maximum survival probability by a factor of 10–100. In general, the survival probability increases with the CN neutron number. However, one can see that, owing to the influence of the neutron closed sub-shell $N = 162$ at the last neutron evaporation step, the $W_{4n}(^{272}\text{Hs}^*)$ $[W_{5n}(^{273}\text{Hs}^*)]$ becomes comparable with $W_{4n}(^{273}\text{Hs}^*)$ $[W_{5n}(^{274}\text{Hs}^*)]$ at $E^*_{\text{CN}} > 30$ MeV $[E^*_{\text{CN}} > 40$ MeV]. The position of the maximum of W_{xn} is shifted to the lower energy with decreasing N. For the isotopes Hs considered, the maxima of W_{xn} are in the following energy intervals: $E^*_{\text{CN}} = 28$–30, 38–41, and 49–52 MeV for the $3n$, $4n$, and $5n$ evaporation channels.

In Figs. 4 and 5, the calculated evaporation residue cross sections agree well with the experimental data within a factor of 2–4. In all reactions, the excitation functions reach the maximum value at the energy around $E^*_{\text{CN}} = V_B + Q$, at which the initial nuclei overcome the Coulomb barrier at the side-by-side orientation. Above this barrier, the evaporation residue cross section decreases owing to the decreasing survival probability. At energy lower than $E^*_{\text{CN}} = V_B + Q$, the cross section is lower because the effective capture cross section and fusion probability (for more symmetric reactions) are small.

In the reactions $^{26}\text{Mg} + ^{248}\text{Cm}$, $^{30}\text{Si} + ^{244}\text{Pu}$, $^{36}\text{S} + ^{238}\text{U}$, and $^{48}\text{Ca} + ^{226}\text{Ra}$ the CN ^{274}Hs* are formed (Fig. 4). Because in the reactions $^{26}\text{Mg} + ^{248}\text{Cm}$ and $^{30}\text{Si} + ^{244}\text{Pu}$ the effective capture cross sections $\sigma^{\text{eff}}_{\text{cap}}$ (Fig. 1) and fusion probabilities P_{CN} are almost the same, their excitation functions are similar

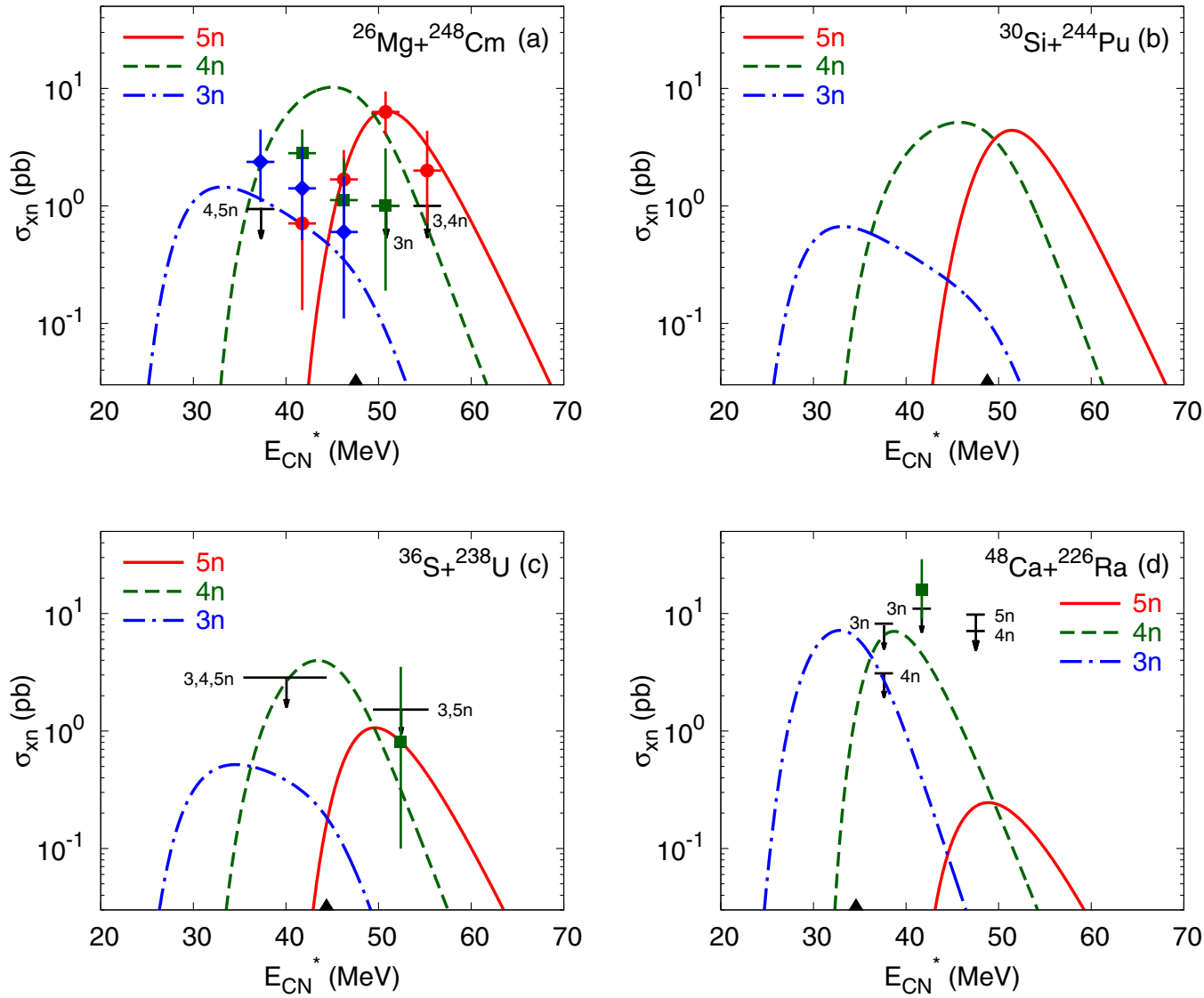

FIG. 4. (Color online) The measured (symbols) and calculated (lines) excitation functions for xn evaporation channels ($x = 3$–5) in the reactions indicated. The $3n$, $4n$, and $5n$ channels are indicated by the dash-dotted, dashed, and solid lines, respectively. The circles, squares, and diamonds represent the experimental data [3,14–17] with errors for the $5n$, $4n$, and $3n$ channels, respectively. The black horizontal lines with arrows are the upper limits of the evaporation residue cross sections in given xn channels, and the black triangles at the energy axis indicate the excitation energy $E^*_{\text{CN}} = V_B + Q$ of the CN. The excitation energies are calculated by using the predictions from the mass table of Ref. [39].

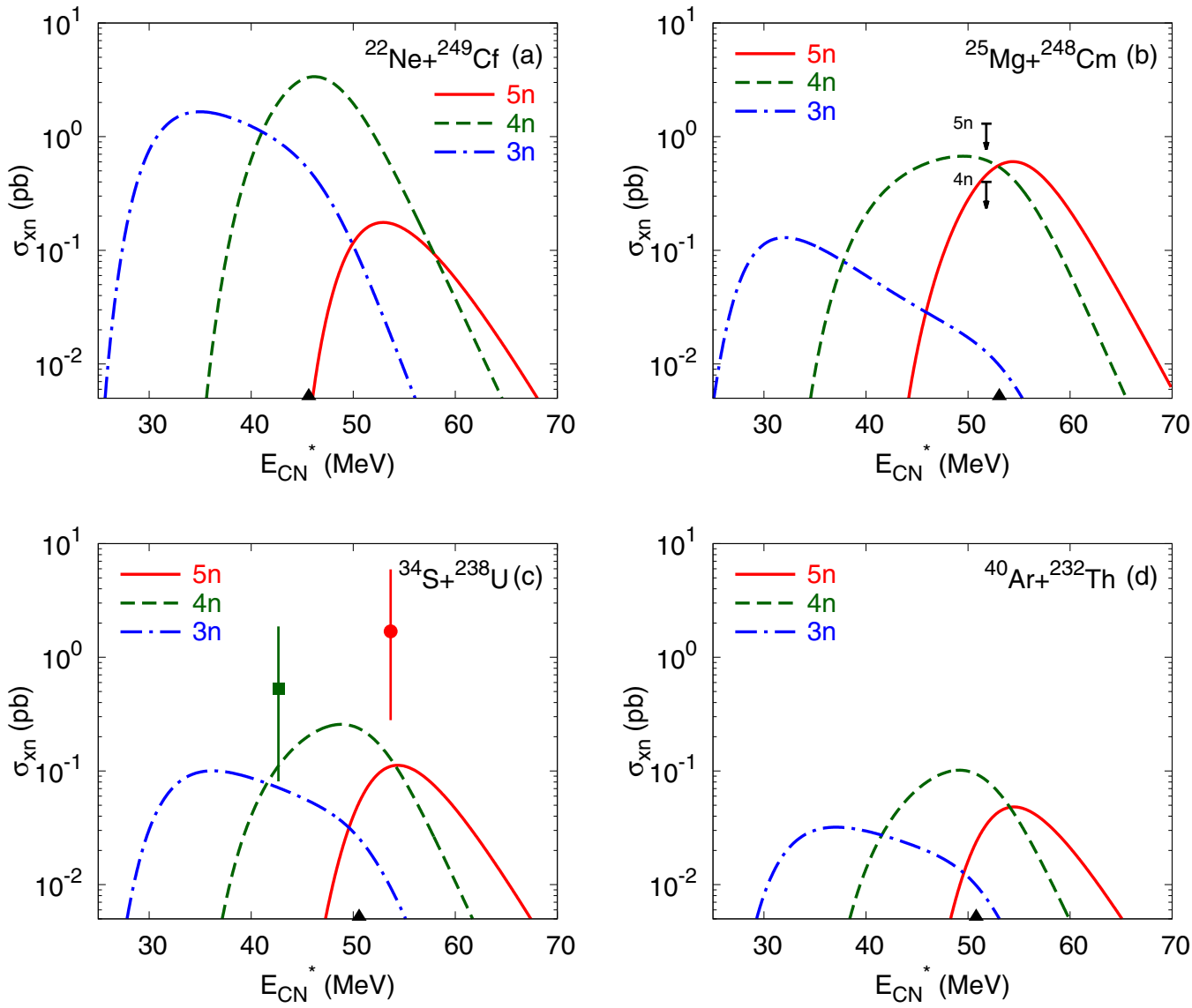

FIG. 5. (Color online) The same as in Fig. 4, but for the reactions indicated. The experimental data are from Refs. [3,15,16].

(Fig. 4). The maximum σ_{3n} and σ_{4n} are at the level of 1 and 10 pb. In these reactions, the maximum yields of the $4n$ and $5n$ channels are comparable at $E^*_{\rm CN}(4n) = 45$ MeV and $E^*_{\rm CN}(5n) = 50$ MeV. In the $^{30}{\rm Si} + ^{244}{\rm Pu}$ reaction, the larger loss in the capture cross section is compensated by the larger gain in the fusion probability compared with the $^{36}{\rm S} + ^{238}{\rm U}$ reaction and $\sigma_{4n}(^{30}{\rm Si} + ^{244}{\rm Pu}) \approx \sigma_{4n}(^{36}{\rm S} + ^{238}{\rm U}) \approx 4$ pb. For the $5n$ channel, the capture cross sections in both reactions are almost the same, but $P_{\rm CN}(^{30}{\rm Si} + ^{244}{\rm Pu}) > P_{\rm CN}(^{36}{\rm S} + ^{238}{\rm U})$ and $\sigma_{5n}(^{30}{\rm Si} + ^{244}{\rm Pu}) \approx 4\sigma_{5n}(^{36}{\rm S} + ^{238}{\rm U})$. Note that for the reaction with ^{36}S the maximum W_{4n} and W_{5n} are at 38 and 49 MeV, respectively, and $V_B + Q = 44.4$ MeV. Therefore, the maximum of σ_{4n} is at 43 MeV and $\sigma_{4n}(^{36}{\rm S} + ^{238}{\rm U}) \approx 4\sigma_{5n}(^{36}{\rm S} + ^{238}{\rm U})$. The $^{48}{\rm Ca} + ^{226}{\rm Ra}$ reaction has $E^*_{\rm CN} = V_B + Q$ lower by about 10–14 MeV compared to other reactions forming $^{274}{\rm Hs}^*$. Thus, the $3n$ channel becomes optimal along with the $4n$ channel: $\sigma_{3n} \approx \sigma_{4n} \approx 7$ pb. The maximum cross sections in the $(3$–$4)n$ channels are more than one order of magnitude larger than the one in the $5n$ channel. In this reaction, the production cross section of ^{272}Hs is also relatively large, about 1 pb.

Although the survival probabilities of the CN are almost equal in the reactions $^{34}{\rm S} + ^{238}{\rm U}$ and $^{40}{\rm Ar} + ^{232}{\rm Th}$, the evaporation residue cross sections are different by a factor about of 2–3.3 because of different capture cross sections (different values of V_B and Q [see Table I]) and fusion probabilities (Fig. 5). Because in these reactions the difference of the fusion probabilities is larger at low energies, the maximum discrepancy of the production cross section occurs in the $3n$ evaporation channel. For the $^{34}{\rm S} + ^{238}{\rm U}$ [$^{40}{\rm Ar} + ^{232}{\rm Th}$] reaction, $\sigma_{4n}/\sigma_{3n} \approx 3$ [$\sigma_{4n}/\sigma_{3n} \approx 3.3$], and $\sigma_{4n}/\sigma_{5n} \approx 2.5$ [$\sigma_{4n}/\sigma_{5n} \approx 2$]. For the $^{22}{\rm Ne} + ^{249}{\rm Cf}$ reaction (Fig. 5), $\sigma_{3n} \approx \sigma_{3n}(^{26}{\rm Mg} + ^{248}{\rm Cm})$, $\sigma_{4n} \approx \frac{1}{3}\sigma_{4n}(^{26}{\rm Mg} + ^{248}{\rm Cm}) \approx 3$ pb, and

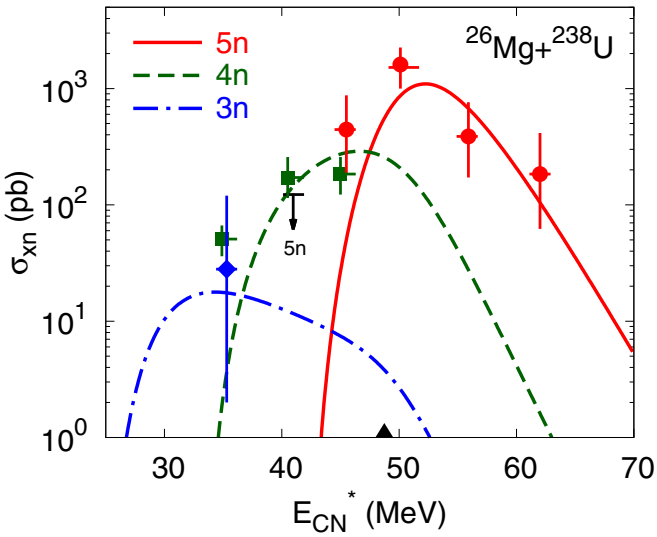

FIG. 6. (Color online) The same as in Fig. 4, but for the indicated reaction. The experimental data are from Ref. [40].

$\sigma_{5n} \approx \frac{1}{30}\sigma_{5n}(^{26}\mathrm{Mg}+^{248}\mathrm{Cm}) \approx 0.2$ pb. For the reactions $^{22}\mathrm{Ne}+^{249}\mathrm{Cf}$ and $^{26}\mathrm{Mg}+^{248}\mathrm{Cm}$, the main discrepancy appears to be attributable to the difference of their survival probabilities. For the $^{22}\mathrm{Ne}+^{249}\mathrm{Cf}$ reaction, the gain in the capture is weaker than the loss in the survival probability owing to the deficit of neutrons in the CN (^{271}Hs). The losses of the capture and survival probabilities in the $^{25}\mathrm{Mg}+^{248}\mathrm{Cm}$ reaction are larger than in the $^{26}\mathrm{Mg}+^{248}\mathrm{Cm}$ reaction. As a result, the strong decrease of the cross sections is found: $\sigma_{3n} \approx \frac{1}{13}\sigma_{3n}(^{26}\mathrm{Mg}+^{248}\mathrm{Cm}) \approx 0.1$ pb and $\sigma_{4n} \approx \frac{1}{14}\sigma_{4n}(^{26}\mathrm{Mg}+^{248}\mathrm{Cm}) \approx 0.7$ pb.

In Fig. 6 we also consider the production cross sections of the Rf isotopes in the $^{26}\mathrm{Mg}+^{238}\mathrm{U}$ reaction. Our calculated results agree with the experimental data within a factor of 2–3, and the ratio of the maxima of the $5n$ channel to the $4n$ channel is well reproduced. One can compare the reactions $^{26}\mathrm{Mg}+^{238}\mathrm{U}$ and $^{30}\mathrm{Si}+^{244}\mathrm{Pu}$, which have almost the same capture cross sections [$V_B + Q(^{26}\mathrm{Mg}+^{238}\mathrm{U}) \approx V_B + Q(^{30}\mathrm{Si}+^{244}\mathrm{Pu}) \approx 49$ MeV] and fusion probabilities [$P_{\mathrm{CN}} \approx 1$]. Because the liquid drop barrier height B_{LD} is larger for the lighter system, the ratio $W_{xn}/W_{(x-1)n}$ is about 10 times larger than in the case of the reaction $^{30}\mathrm{Si}+^{244}\mathrm{Pu}$. As a result, for the ^{264}Rf CN the W_{xn} does not fall down strongly as in the case of the ^{274}Hs, and in the $^{26}\mathrm{Mg}+^{238}\mathrm{U}$ reaction the $5n$ channel dominates with the cross section 1 nb, $\sigma_{5n}/\sigma_{4n} \approx 3.3$ and $\sigma_{5n}/\sigma_{3n} \approx 50$.

The ratio of the cross sections in the neighboring evaporation channels depends on the change of $\sigma_{\mathrm{cap}}^{\mathrm{eff}} P_{\mathrm{CN}}$ and W_{xn} with E_{CN}^*. While the value of $\sigma_{\mathrm{cap}}^{\mathrm{eff}} P_{\mathrm{CN}}$ generally increases with excitation energy of the CN, the survival probability decreases. These opposite trends in Eq. (6) result in larger width of the excitation function in the $3n$ evaporation channel. Also, the shape of this function visibly deviates from the Gaussian (Figs. 4, 5, and 6).

IV. SUMMARY

Within the DNS model we studied the production of isotopes of $^{266-271}$Hs in various reactions at near- and sub-barrier energies. Figures 4 and 5 show our main calculated results of the evaporation residue cross sections. Although there are many uncertainties to calculate the evaporation residue cross section, the model seems to be working reasonably. The calculated cross sections agree with experimental data within a factor of 2–4. For the reactions leading to the formation of the same CN, the production of isotopes strongly depends on the entrance channel effects [deformation effect, Q-value effect, the entrance charge (mass) asymmetry]. The main distinction is because of the different capture and fusion probabilities. We were able to make some predictions for xn channels. The maximum $\sigma_{3n} \approx 7$ pb at $E_{\mathrm{CN}}^* = 33$ MeV was found for the $^{48}\mathrm{Ca}+^{226}\mathrm{Ra}$ reaction. The relatively large cross sections $\sigma_{3n} \approx 1$ pb at the energy 33 MeV were predicted in the reactions $^{26}\mathrm{Mg}+^{248}\mathrm{Cm}$ and $^{30}\mathrm{Si}+^{244}\mathrm{Pu}$. For the $^{36}\mathrm{S}+^{238}\mathrm{U}$ reaction, the optimal production channel is $4n$ with the cross section of about 4 pb at energy 42 MeV. For this reaction, $\sigma_{3n} = 0.5$ pb at $E_{\mathrm{CN}}^* = 35$ MeV. At sub-barrier energies the excitation functions in the $3n$ channel are wider than those in the $4n$ and $5n$ evaporation channels and their shapes strongly deviate from the Gaussian.

ACKNOWLEDGMENTS

This work is supported by the Rare Isotope Science Project of Institute for Basic Science funded by Ministry of Science, ICT, and Future Planning and National Research Foundation of Korea (Grant No. 2013M7A1A1075766). The support of the Russian Foundation for Basic Research (Moscow) is greatly acknowledged.

[1] Yu. Ts. Oganessian, J. Phys. G **34**, R165 (2007).
[2] Yu. Ts. Oganessian *et al.*, Phys. Rev. Lett. **104**, 142502 (2010); Phys. Rev. C **87**, 014302 (2013); **87**, 054621 (2013).
[3] Yu. Ts. Oganessian *et al.*, Phys. Rev. C **87**, 034605 (2013).
[4] S. Hofmann, Rep. Prog. Phys. **61**, 639 (1998); Lect. Notes Phys. **764**, 203 (2009); Radiochim. Acta **99**, 405 (2011).
[5] S. Hofmann and G. Münzenberg, Rev. Mod. Phys. **72**, 733 (2000).
[6] S. Hofmann *et al.*, Eur. Phys. J. A **32**, 251 (2007); **48**, 62 (2012).
[7] K. Morita *et al.*, Eur. Phys. J. A **21**, 257 (2004); J. Phys. Soc. Jpn. **73**, 2593 (2004); **76**, 043201 (2007).
[8] L. Stavsetra, K. E. Gregorich, J. Dvorak, P. A. Ellison, I. Dragojević, M. A. Garcia, and H. Nitsche, Phys. Rev. Lett. **103**, 132502 (2009); Ch. E. Düllmann *et al.*, *ibid.* **104**, 252701 (2010); J. M. Gates *et al.*, Phys. Rev. C **83**, 054618 (2011).
[9] J. Peter *et al.*, Nucl. Phys. A **734**, 192 (2004).

[10] S. Cwiok *et al.*, Nucl. Phys. A **410**, 254 (1983); Z. Patyk *et al.*, *ibid.* **502**, 591 (1989); Z. Patyk and A. Sobiczewski, *ibid.* **533**, 132 (1991).
[11] P. Möller, J. R. Nix, and W. J. Swiatecki, Nucl. Phys. A **469**, 1 (1987); **492**, 349 (1989); P. Möller and J. R. Nix, *ibid.* **549**, 84 (1992).
[12] Yu. A. Lazarev *et al.*, Phys. Rev. Lett. **73**, 624 (1994).
[13] S. Hofmann *et al.*, Eur. Phys. J. A **14**, 147 (2002).
[14] J. Dvorak *et al.*, Phys. Rev. Lett. **100**, 132503 (2008).
[15] R. Graeger *et al.*, Phys. Rev. C **81**, 061601 (2010).
[16] K. Nishio *et al.*, Phys. Rev. C **82**, 024611 (2010).
[17] J. Dvorak *et al.*, Phys. Rev. C **79**, 037602 (2009).
[18] G. G. Giardina, S. Hofmann, A. I. Muminov, and A. K. Nasirov, Eur. Phys. J. A **8**, 205 (2000); G. G. Giardina, F. Hanappe, A. I. Muminov, A. K. Nasirov, and L. Stuttgé, Nucl. Phys. A **671**, 165 (2000); A. K. Nasirov *et al.*, *ibid.* **759**, 342 (2005); H. Q. Zhang *et al.*, Phys. Rev. C **81**, 034611 (2010); A. K. Nasirov, G. Mandaglio, G. G. Giardina, A. Sobiczewski, and A. I. Muminov, *ibid.* **84**, 044612 (2011).
[19] Z. H. Liu and J. D. Bao, Phys. Rev. C **74**, 057602 (2006).
[20] N. Wang, J. Tian, and W. Scheid, Phys. Rev. C **84**, 061601(R) (2011).
[21] V. V. Sargsyan, G. G. Adamian, N. V. Antonenko, W. Scheid, and H. Q. Zhang, Phys. Rev. C **84**, 064614 (2011); **91**, 014613 (2015).
[22] N. Wang, E. G. Zhao, W. Scheid, and S. G. Zhou, Phys. Rev. C **85**, 041601(R) (2012); N. Wang, E. G. Zhao, and W. Scheid, *ibid.* **89**, 037601 (2014).
[23] L. Zhu, Z. Q. Feng, C. Li, and F. S. Zhang, Phys. Rev. C **90**, 014612 (2014); Z. Q. Feng, G. M. Jin, J. Q. Li, and W. Scheid, *ibid.* **76**, 044606 (2007).
[24] V. V. Volkov, Phys. Rep. **44**, 93 (1978); Izv. Akad. Nauk SSSR, Ser. Fiz. **50**, 1879 (1986); *Nuclear Reactions of Deep Inelastic Transfers* (Energoizdat, Moscow, 1982); in *Treatise on Heavy-Ion Science*, edited by D. A. Bromley (Plenum, New York, 1989), Vol. 8, p. 255; Part. Nucl. **35**, 797 (2004).
[25] G. G. Adamian, N. V. Antonenko, and W. Scheid, *Clustering Effects Within the Dinuclear Model*, Lecture Notes in Physics, edited by C. Beck (Springer, Berlin, 2012), Vol. 848, p. 165.
[26] C. Y. Wong, Phys. Rev. Lett. **31**, 766 (1973).
[27] A. B. Migdal, *Theory of Finite Fermi Systems and Application to Atomic Nuclei* (Nauka, Moscow, 1967).
[28] G. G. Adamian, N. V. Antonenko, R. V. Jolos, S. P. Ivanova, and O. I. Melnikova, Int. J. Mod. Phys. E **05**, 191 (1996).
[29] A. S. Zubov, G. G. Adamian, N. V. Antonenko, S. P. Ivanova, and W. Scheid, Phys. Rev. C **68**, 014616 (2003).
[30] R. A. Kuzyakin, V. V. Sargsyan, G. G. Adamian, N. V. Antonenko, E. E. Saperstein, and S. V. Tolokonnikov, Phys. Rev. C **85**, 034612 (2012).
[31] P. Reiter *et al.*, Phys. Rev. Lett. **82**, 509 (1999); **84**, 3542 (2000).
[32] G. G. Adamian, N. V. Antonenko, W. Scheid, and V. V. Volkov, Nucl. Phys. A **627**, 361 (1997); **633**, 409 (1998); G. G. Adamian, N. V. Antonenko, and W. Scheid, *ibid.* **678**, 24 (2000).
[33] K.-H. Schmidt *et al.*, in *Proceedings of the International Symposium on Physics and Chemistry of Fission, Jülich, 1979* (IAEA, Vienna, 1980), Vol. 1, p. 407; P. Armbruster, Annu. Rev. Nucl. Part. Sci. **35**, 135 (1985); G. Münzenberg, Rep. Prog. Phys. **51**, 57 (1988); K.-H. Schmidt and W. Morawek, *ibid.* **54**, 949 (1991).
[34] D. L. Hill and J. A. Wheeler, Phys. Rev. **89**, 1102 (1953).
[35] E. A. Cherepanov, A. S. Iljinov, and M. V. Mebel, J. Phys. G **9**, 931 (1983).
[36] A. S. Zubov, G. G. Adamian, N. V. Antonenko, S. P. Ivanova, and W. Scheid, Phys. Rev. C **65**, 024308 (2002).
[37] R. Vandenbosch and J. R. Huizenga, *Nuclear Fission* (Academic Press, New York, 1973).
[38] A. J. Sierk, Phys. Rev. C **33**, 2039 (1986).
[39] P. Möller, J. R. Nix, W. D. Myers, and W. J. Swiatecki, At. Data Nucl. Data Tables **59**, 185 (1995).
[40] J. M. Gates *et al.*, Phys. Rev. C **77**, 034603 (2008).